# Silk Fluorescence Collimator for Ultrasensitive Humidity Sensing and Light-Harvesting in Semitransparent Dye-Sensitized Solar Cells

Hu, Fan; Liu, Wenzhe; Li, Weifeng; Xu, Zijie; Diao, Ying Ying; Lin, Nai Bo; Guo, Wenxi; Shi, Lei; van Esch, Jan H.; Liu, Xiang Yang

**Citation (APA)**
Hu, F., Liu, W., Li, W., Xu, Z., Diao, Y. Y., Lin, N. B., Guo, W., Shi, L., van Esch, J. H., & Liu, X. Y. (2019). Silk Fluorescence Collimator for Ultrasensitive Humidity Sensing and Light-Harvesting in Semitransparent Dye-Sensitized Solar Cells. *Small*, *15*(13), Article 1804171. https://doi.org/10.1002/smll.201804171

**Important note**
To cite this publication, please use the final published version (if applicable).
Please check the document version above.

**COMMUNICATION**

Fluorescence

NANO · MICRO

small

www.small-journal.com

Check for updates

# Silk Fluorescence Collimator for Ultrasensitive Humidity Sensing and Light-Harvesting in Semitransparent Dye-Sensitized Solar Cells

*Fan Hu, Wenzhe Liu, Weifeng Li, Zijie Xu, Ying Ying Diao, Nai Bo Lin, Wenxi Guo, Lei Shi, Jan H. van Esch, and Xiang Yang Liu\**

This work examines the self-collimation effect of silk materials on fluorescence emission/detection. A macroscopic regulation strategy, coupled with meso-reconstruction and meso-functionalization, is adopted to amplify the fluorescence emission of organic fluorescent dyes (i.e., Rhodamine 6G (R6G)) using silk photonic crystal (PC) films. The fluorescence emission can be linearly enhanced or inhibited by a PC as a result of the photonic bandgap coupling with the excitation light and/or emission light. Depending on the design of the silk fluorescence collimator, the emission can reach 49.37 times higher than the control. The silk fluorescence collimator can be applied to achieve significant benefits: for instance, as a humidity sensor, it provides good reproducibility and a sensitivity of 28.50 a.u./% relative humidity, which is 80.78 times higher than the sensitivity of the control, and as a novel curtain, it raises the energy conversion efficiency of the semitransparent dye-sensitized solar cells (DSSCs) by 16%.

Fluorescent dye-based devices are widely applied in many fields, such as fluorescence light sources, adjustable fluorescence devices, and fluorescence-based bioassays.[1] The intensity of fluorescence emission is a vital parameter for fluorescent devices. To efficiently enhance fluorescence emission, several highly sensitive analytical techniques have been developed, such as fluorescence resonance energy transfer, photoinduced fluorescence enhancement, and the surface plasmon resonance of metal nanoparticles.[2] However, due to the rigorous operating conditions and high-cost/complicated fabrication process involved in the abovementioned techniques,[3] the low fluorescence emission efficiency of organic fluorescent dyes remains unchanged in the practical implications and applications of fluorescent dye-based devices. Therefore, there is a need to introduce a more practical strategy to overcome this barrier.

Silks, which are produced by Bombyx mori silkworms, are typical natural fibrous materials with extraordinary mechanical performance, biocompatibility, and excellent optical properties.[4] As a typical class of flexible materials, fluorescent silk materials have attracted significant attention for fabric production, flexible/implantable electronics, and biomedical applications.[5] As the macroscopic performance or functionality of soft materials can be related with the interaction, correlation length, and structural ordering at the mesoscale,[6] the coupling of fluorescence emission from doped Rhodamine 6G (R6G) silk fibroin (SF) films with the inverse opal photonic crystal (PC) structure will be examined. Notably, the regulating strategy is not limited to the silk materials. Like the slow photon effect,[7] the self-collimation effect is originated from the unique property of structure controlling and manipulating light.

In this work, we demonstrated a simple strategy that can control the mesoscale structures and architectures of soft materials to achieve extraordinary fluorescence-emission performance, which may lead to the next generation of fluorescence detection/imaging technologies. In addition, few reports have investigated fluorescence enhancement by adjusting the emission mode through a mesoscopic regulation strategy. Importantly, we highlight that silk PC films can serve as a "self-collimator" by greatly amplifying fluorescence emission or

F. Hu, W. Li, Z. Xu, Dr. N. B. Lin, Dr. W. Guo, Prof. X. Y. Liu
Research Institute for Biomimetics and Soft Matter
College of Materials
College of Physical Science and Technology
Fujian Provincial Key Laboratory for Soft Functional Materials Research
Xiamen University
Xiamen 361005, China
E-mail: liuxy@xmu.edu.cn, phyliuxy@nus.edu.sg
F. Hu, Prof. J. H. van Esch
Advanced Soft Matter Group
Department of Chemical Engineering
Delft University of Technology
Van der Maasweg 9, 2629 HZ Delft, The Netherlands
W. Liu, Dr. L. Shi
Department of Physics
Key Laboratory of Micro- and Nano-Photonic Structures
(Ministry of Education)
and State Key Laboratory of Surface Physics
Fudan University
Shanghai 200433, China
Dr. Y. Y. Diao, Prof. X. Y. Liu
Department of Physics
National University of Singapore
2 Science Drive 3, 117542 Singapore, Singapore

The ORCID identification number(s) for the author(s) of this article can be found under https://doi.org/10.1002/smll.201804171.

ADVANCED
SCIENCE NEWS
www.advancedsciencenews.com

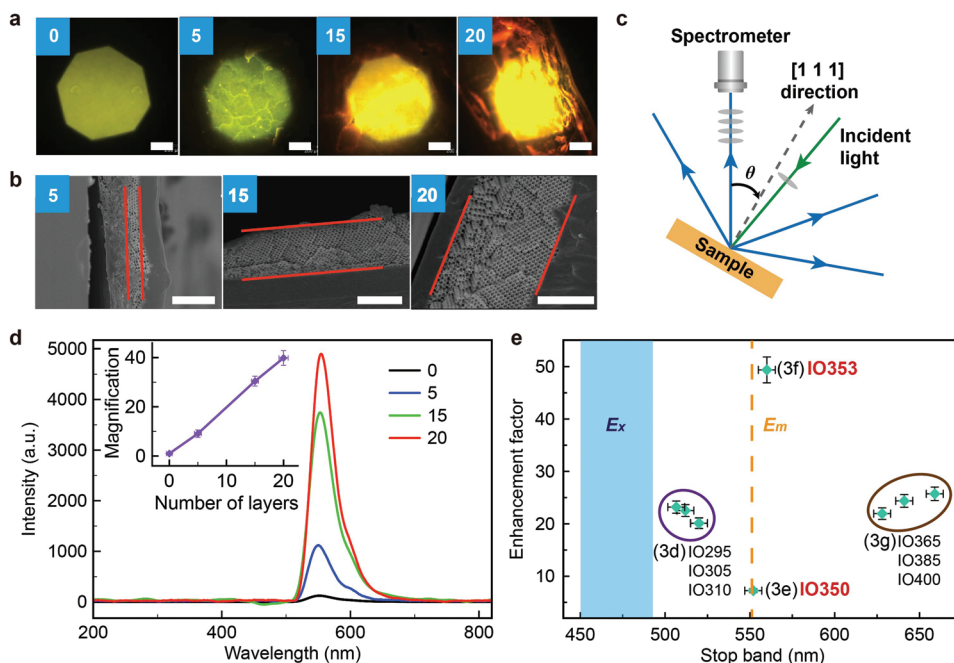NANO · MICRO
small
www.small-journal.com

**Figure 1.** Fluorescence emission adjusted by silk PCs. a) Fluorescence microscopy images of the control (0 layer) and PC films (IO500) with 5 layers, 15 layers, and 20 layers; scale bar: 500 µm. b) Scanning electron microscopy (SEM) images of the fluorescent silk PCs (IO500); scale bar: 2 µm. c) Schematic of the optical setup. The incident light is focused on the [1 1 1] direction, and the emission is detected by a spectrometer at the angle $\theta$. Here, the spectrometer is set up at $\theta = 0°$ through a fluorescence microscope. Note that the detected angle range is $\theta = -30°$ to $30°$. The numerical aperture of the objective lens of the microscope is 0.5. The maximal half-angle of the cone of light that can enter or exit the objective lens is $30°$ (= arccos 0.5). d) Fluorescence spectra of R6G-doped silk PCs and the control ($E_x$, $\lambda$: 450–490 nm, $E_m$, $\lambda$: 553 nm). Inset: The amplification of the fluorescence intensity increases as the number of layers of the inverse opal structure increases. e) Comparison of the fluorescence intensity of silk PCs with different stopbands, together with the excitation light ($E_x$, blue shadow region) and the normalized fluorescence emission of R6G ($E_m$, orange dashed line). The enhancement factor refers to the ratio of fluorescence intensity of silk PC films to that of the control (the solid silk film sample doped with R6G). The stopbands of silk PC films are centered at 506.6, 512, 520, 553, 560, 628, 641, and 659 nm. Error bars refer to the standard deviations of more than five independent measurements. Note that the surface areas and the quantities of both the SF materials and R6G in all samples with different structures remain the same.

improving fluorescence detection. Finally, as two examples of applied biofriendly devices, a silk-based fluorescence humidity sensor and an empowered fluorescence curtain for semitransparent dye-sensitized solar cells (DSSCs) are demonstrated.

To fabricate the fluorescent SF materials, SF solutions/films were meso-doped with the dye R6G (Figure S1, Supporting Information). Subsequently, R6G molecules were uniformly distributed throughout the SF films by mesoscopic doping because of the hydrogen-bonding interactions between the SF and R6G molecules at the mesoscopic scale.[8] This approach avoids the aggregation-caused quenching of R6G (Figure S2, Supporting Information). R6G-doped silk PCs were obtained by 1) preparing polystyrene (PS) colloidal crystals by the Czochralski method, 2) infiltrating the colloidal crystals with an R6G-doped silk solution, and 3) removing the PS templates (Supporting Information). The layer number of the PCs can be adjusted by controlling the withdrawal rate $v$ (Figure S3, Supporting Information).[9] As shown in **Figure 1**a–d, the fluorescence spectra of R6G-doped silk PCs with 0, 5, 15, and 20 layers were measured at $\theta = 0°$ (the control refers to the R6G-doped SF films without a PC structure (0 layer), and silk PCs were fabricated using PS spheres with a diameter of 500 nm). Note that in each series of comparative experiments, the surface areas and the quantities of both the SF materials and R6G in all samples

with different structures remain the same (Supporting Information). The emission peak ($\lambda_{em} = 553$ nm) does not overlap with the reflection peak of the silk PCs ($\lambda_{PC} = 885$ nm). Consequently, the fluorescence emission of the SF films increases linearly with the PC layer number, and the fluorescence emission is amplified by 40 times (with 20 layers). This outcome is also applicable to silk PCs of different lattice constants and different fluorescent dyes (Figure S4, Supporting Information). After optimizing the correlation between the photonic bandgap (PBG) and fluorescent emission, we noticed that ten-layer R6G-doped silk PCs can increase the self-fluorescence emission by 50 times (Figure 1e).

To obtain the maximum fluorescence enhancement, the structure factors of the silk PCs were optimized by adjusting the wavelength corresponding to the PBG while keeping the number of silk PC layers and amounts of R6G/SF constant. The PBG wavelengths of the silk PCs were tuned by changing the diameter of the PS spheres (Supporting Information). The different cases were named according to the following rule: silk PC films prepared by PS spheres with a diameter of 353 nm were named IO353 (Figure 1e). For the above case (IO353), the blue band edge of the reflection peak partly overlaps with the emission peak of the R6G-doped silk PCs (Figure S5, Supporting Information). In this study, compared with the control,
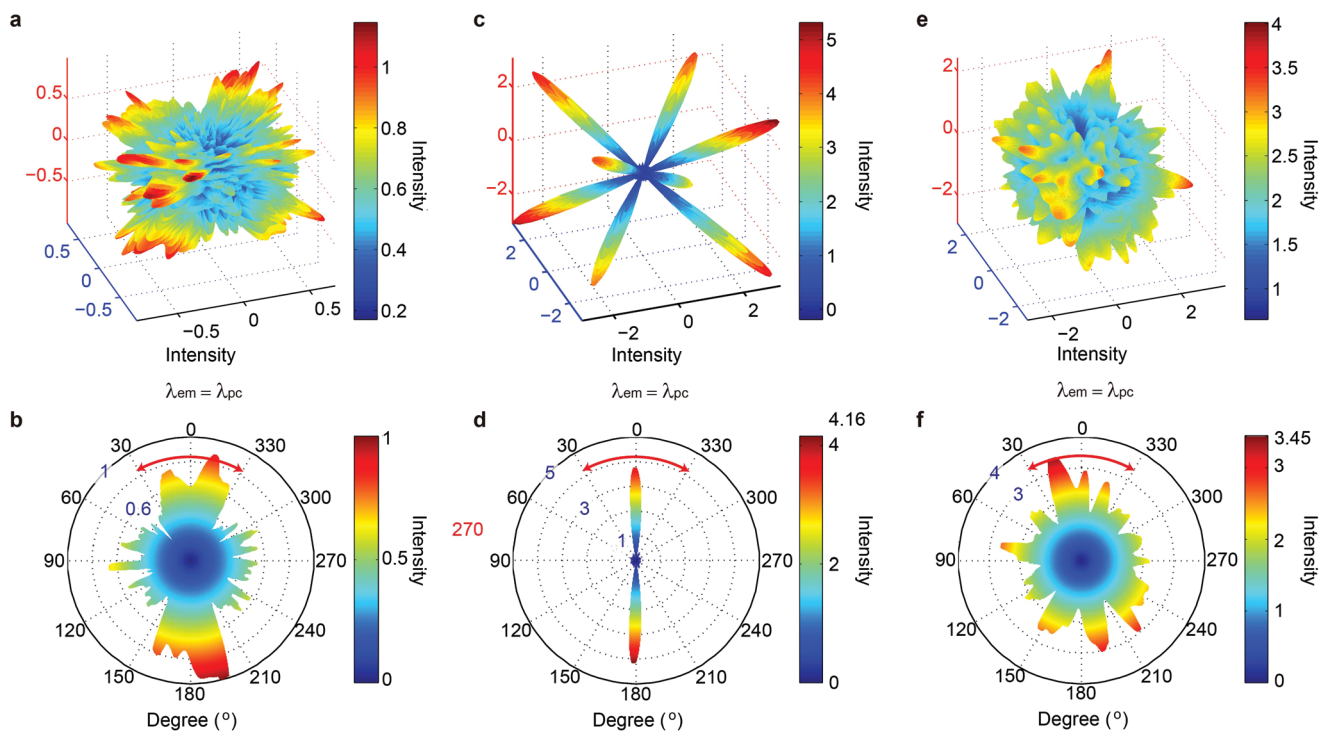
**Figure 2.** FDTD simulation of fluorescence emission. The fluorescence emission in different silk PCs was simulated by the FDTD method (Supporting Information). The light emits at the wavelength of $\lambda_{em}$, and the wavelength corresponding to the PBG structure is $\lambda_{PC}$. a,c,e) 3D FDTD simulation of fluorescence emission when a) $\lambda_{em} = \lambda_{PC}$, c) $\lambda_{em} < \lambda_{PC}$, and e) $\lambda_{em} > \lambda_{PC}$. b,d,f) 2D vertical sections of FDTD simulations of fluorescence emission when b) $\lambda_{em} = \lambda_{PC}$, d) $\lambda_{em} < \lambda_{PC}$, and f) $\lambda_{em} > \lambda_{PC}$.

IO353 was found to achieve the greatest enhancement in fluorescence emission by a factor of 49.37 (detected at $\theta = 0°$). The effect leading to the optimal fluorescence enhancement is illustrated by the finite-difference time-domain (FDTD) simulations in **Figure 2**. When the wavelength of fluorescence emission ($\lambda_{em}$) overlaps with the wavelength of the PBG ($\lambda_{PC}$) ($\lambda_{em} = \lambda_{PC}$, Figure 2a,b), the fluorescence emission along the <1 1 1> directions of the silk PCs is blocked due to Bragg reflections. As a result, much less fluorescence emission is detected at $\theta = 0°$, as it escapes from other angles.[10] Nevertheless, when $\lambda_{em} < \lambda_{PC}$ (Figure 2c,d), the situation is completely different. In the case of $\lambda_{em} < \lambda_{PC}$, the emitted light $\lambda_{em}$ is not Bragg diffracted from the lattice planes at $\theta = 0°$, but instead encounters Bragg diffraction at higher angles. Hence, more light is channeled and confined to the allowed directions, e.g., $\theta = 0°$, due to the low state intensity at the band edge. This effect leads to enhanced fluorescence emission at the blue band side of the PCs at $\theta = 0°$, which is referred to as the "self-collimation" effect of fluorescence emission from silk PCs. However, when the PBG shifts toward shorter wavelengths ($\lambda_{em} > \lambda_{PC}$, Figure 2e,f), the emitted light does experience internal diffraction at higher angles. Therefore, no enhancement is observed.

The effect of the PBG of functionalized silk PCs on fluorescence emission is more complicated than the three cases shown in Figure 2 and needs further clarification. In fact, all of the seven cases summarized in Figure S6 in the Supporting Information may occur. As the reflection peak corresponding to the PBG ("PC," red) shifts from the shorter wavelength of the excitation peak ("$E_x$," blue) to the longer wavelength of the

emission peak ("$E_m$," green), the self-fluorescence intensity can be influenced by the silk PCs in different manners. Note that although these cases have exceptions, they are useful guidelines for understanding how common fluorescence emission is coupled with PC properties.

To examine the implication of the "self-collimation" effect, the functionalized silk PC films were applied to develop a type of biocompatible fluorescent silk PC humidity sensor with high sensitivity. According to Figure S7 in the Supporting Information, silk PCs (IO353) display a reflection peak redshift of ≈20 nm as the relative humidity (RH) increases from 30% to 88%. Here, humidity changes lead to cyclic contractions of the SF materials,[11] giving rise to the variation in "$a$" (the lattice parameter of open spheres in the silk PCs). At a higher humidity level, the swelling of SF results in the expansion of the silk shells (with increasing "$a$"), which caused the redshift in the reflection peak ("PC," red, **Figure 3**a). As the reflection peak consequently moves far away from the emission peak ("$E_m$," green), the fluorescence emission of the silk PC at $\lambda_{em}$ in turn decreases according to the "self-collimation" effect (Figure 3b). In contrast, when the humidity is lowered, the shrinking of SF occurs with the contraction of the silk shells (with decreasing "$a$"); therefore, the fluorescence emission of the silk PC increases with the blueshift in the PBG. The humidity responses of the fluorescence signal of silk PCs are dependent on the PBG shifts of the silk PCs.

The fluorescence intensity of silk PCs (IO353, with a ten-layer PC structure) was measured in one homemade humidity chamber ($E_x$, $\lambda$: 450–490 nm; $E_m$, $\lambda$: 553 nm). Figure 3c depicts
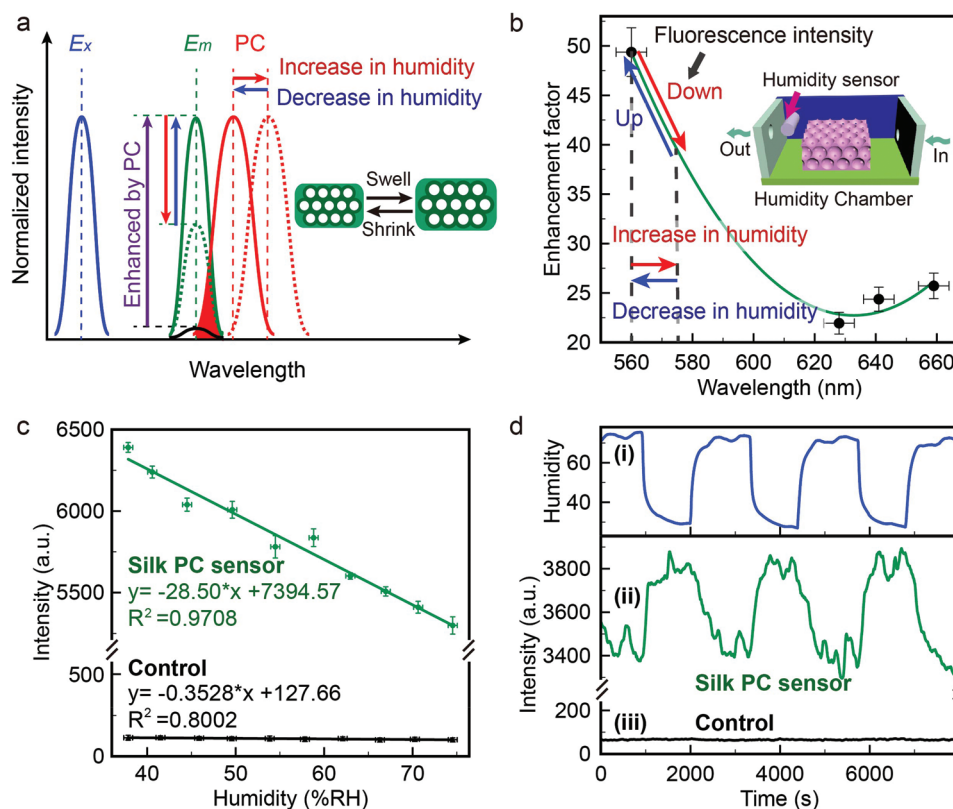
**Figure 3.** Biocompatible silk PC-based humidity sensor. a) Schematic of tuning the fluorescence intensity by the PBG shift due to the humidity changes. Compared with that of the control (black), the fluorescence emission of a silk PC ("$E_m$," green) with the optimized PC structure can be enhanced by dozens of times at the same incident light ("$E_x$," blue). The shifts in the reflection peak ("PC," red) indicate the shifts in the PBG position of the silk PCs. Inset: Schematic of the swelling/shrinking of SF shells. b) Schematic of the trend prediction of the fluorescence intensity of silk PCs with different stopbands. The enhancement factor refers to the ratio of fluorescence intensity of silk PC films to that of the control. The stopbands of silk PC films are centered at 560, 628, 641, and 659 nm. Inset: Schematic of a humidity-controlled chamber. c) Fluorescence emission at different humidity levels for a fluorescent silk film without a PC structure (black, as the control) and a fluorescent silk PC film (green) with an integral time of 1 s. d) Fluorescence measurement (integral time: 0.5 s) of the biocompatible humidity sensor with rapid changes in humidity. (i) Humidity logger data (blue) compared with the corresponding fluorescence shifts of (ii) fluorescent silk PCs (green) and (iii) the fluorescent film sample without the PC structure (black). Error bars refer to standard deviations from at least five independent measurements. Note that the surface areas and the quantities of both the SF materials and R6G in all samples with different structures remain the same.

the linearly declining trend in the fluorescence intensity of silk PCs in response to the humidity decreasing from 37% to 74% RH, while little change was exhibited by the control. As illustrated in **Table 1**, the silk PC sensor produces an improved sensitivity of 28.50 a.u./% RH (80.78 times higher than the control), with an increased linearity of 97.08% and a decreased relative

standard deviation of 0.006559 (15.95 times lower than the control). Figure 3d reveals that the fluorescence intensity shifts of the silk PC sensor (blue) are reversible and stable (humidity: 28–75% RH), whereas the control (black) displays almost no response. The high sensitivity, rapid response, and excellent reproducibility of silk PC-based humidity sensing enable it to acquire highly accurate experimental information about humidity in real time. Due to the biocompatibility of silk materials, silk PC-based humidity sensors can be adopted in various biological environments. Moreover, silk PCs can be recombined with other functional molecules to develop various sensors for in-line monitoring, such as insulin/glucose monitoring.

As another example, we took advantage of the "self-collimation" effect of R6G-doped silk PCs (IO353) to enhance the energy conversion efficiency (ECE) of semitransparent DSSCs. Due to the high visible transmission, semitransparent DSSCs are a good option in smart windows/binds for future eco-buildings,[12] which allow converting outdoor sunlight directly into electricity without jeopardizing the basic functions of windows. Nevertheless, DSSCs are of low ECE. In this regard, the
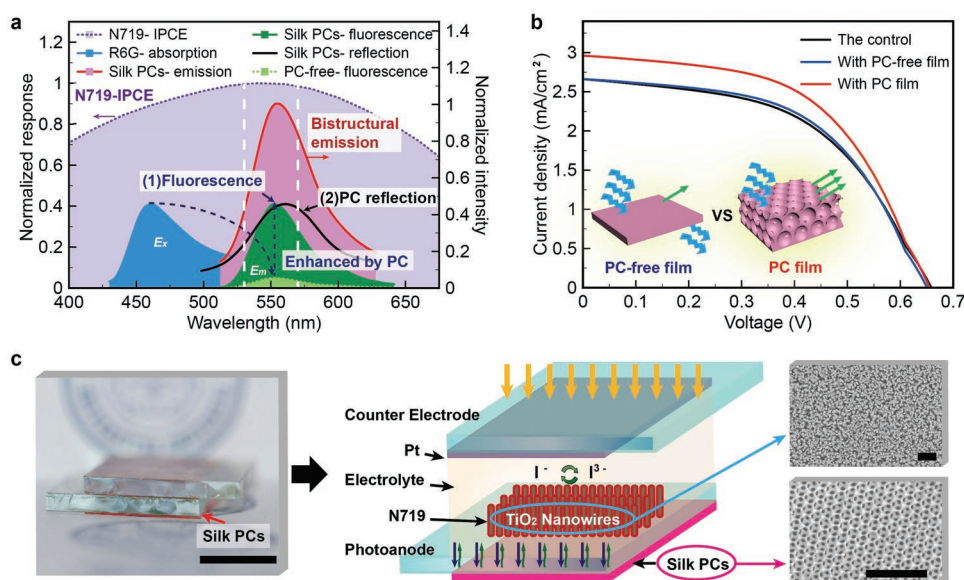
**Table 1.** Performance of humidity sensor.

| Performance | Control | Silk PC sensor |
|---|---|---|
| Sensitivity (37–74% RH) [a.u./% RH][a] | 0.3528 | 28.50 (Improved by 80.78 times) |
| Linearity [%][b] | 80.02 | 97.08 |
| Relative standard deviation (Std. deviation [a.u.])[c] | 0.1046 (12.01) | 0.006559 (38.47) (Lowered by 15.95 times) |

[a]Sensitivity: the ratio of the change in absolute value of the output fluorescence signal to the input relative humidity signal; [b]Linearity: the fitting degree of a line-fitting equation; [c]Relative standard deviation: the ratio of the average standard deviation of all measured data to the maximum change value of fluorescence intensity. All average values are obtained from more than five measurements.

**ADVANCED
SCIENCE NEWS**

www.advancedsciencenews.com

NANO · MICRO

**small**

www.small-journal.com

**Figure 4.** Enhancement of ECE of semitransparent DSSCs by fluorescent silk PCs. a) Schematic of how extra light transmitted through semitransparent DSSCs can be efficiently reused by dye N719 via bistructural emission effect. The bistructural emission (red) denotes a couple of (1) enhanced fluorescence emission spectrum (dark green) and (2) PC reflection spectrum (black), which are exactly overlapped with the incident photo-to-current conversion efficiency (IPCE) cure of dye N719 (grape); the fluorescence emission of silk PC films (dark green) is enhanced by PC structure, compared with silk solid film without PC structure (light green). b) $J$–$V$ curves of the DSSCs with nothing (the control), fluorescent silk solid film (with PC-free film), and fluorescent silk PC film (with PC film). Inset: Schematic of the comparison of fluorescence emission of the fluorescent silk solid film (PC-free film) and the fluorescent silk PC film (PC film). c) Digital photograph (left; scale bar, 1 cm) and illustration (middle) of the DSSC attached with fluorescent silk PC film, in addition to SEM images of the oriented titanium dioxide ($TiO_2$) nanowires (upper right, scale bar, 2 µm) and the silk PCs (bottom right, scale bar, 2 µm). The fluorine-doped tin oxide (FTO) glasses with dye-sensitized $TiO_2$ nanowires were employed as photoanode, while semitransparent platinized FTO glasses were utilized as counter electrode (Supporting Information). Notice that the surface area and the quantities of both SF materials and R6G of all samples of different structures remain the same.

functionalized silk PC films were applied to enhance the ECE of DSSCs. This can be implemented by integrating the silk PC–enhanced fluorescence films into DSSCs.

This integration utilizes the transmitted light in two manners to further enhance the ECE of semitransparent DSSCs. As shown in **Figure 4**a, the dye N719 used in DSSCs can achieve the highest incident photo-to-current conversion efficiency (IPCE) value once incident light occurs at the wavelength of 530–570 nm,[13] labeled as "highlight wavelength band." Here, the idea is, apart from offering reflected light by PCs as most articles reported, to convert the transmitted solar energy from the transmitted light of shorter wavelengths to the "highlight wavelength band" by fluorescence. Furthermore, the fluorescence intensity will be greatly enhanced at $\theta = 0°$ by the silk PC "self-collimators." Therefore, by taking advantage the PC "self-collimation" effect, we can in principle obtain the effective collective angle so as to pursue a higher ECE of DSSCs.[14]

The design of the apparatus is given in Figure 4c. A fluorescent silk PC film was placed tightly against the photoanode of a backside-illuminated DSSC. Figure 4b displays the comparison of current density ($J$)–voltage ($V$) curves, and the photovoltaic parameters are listed in **Table 2**. It follows that the current intensity ($J_{SC}$), the open-circuit voltage ($V_{OC}$), and the fill factor (FF) of the hybrid fluorescent silk PC–enhanced DSSCs are 2.941 mA cm$^{-2}$, 0.675 V, and 59.5%, respectively, yielding an ECE of 1.182%, which is 16% higher than the control and the DSSCs having the R6G-functionalized silk films without PC structure (1.021%, 1.046%).

In conclusion, we demonstrated that the coupling of the PC structure with R6G dye–functionalized silk materials gives rise to the enhancement/inhibition of fluorescence emission. By shifting the PBG position, the self-fluorescence emission of silk PCs can be applied as a key component in biocompatible humidity sensors that offer an increased sensitivity of

**Table 2.** Photovoltaic parameters of DSSCs.

| Sample | $J_{SC}$ [mA cm$^{-2}$][a] | $V_{OC}$ [V][b] | FF [%][c] | ECE [%][d] | Relative ECE[e] |
|---|---|---|---|---|---|
| The control | 2.667 ± 0.006 | 0.677 ± 0.001 | 56.5 ± 0.2 | 1.021 ± 0.005 | 1.00 |
| With PC-free film | 2.661 ± 0.005 | 0.672 ± 0.001 | 58.5 ± 0.5 | 1.046 ± 0.009 | 1.02 |
| With PC film | 2.941 ± 0.019 | 0.675 ± 0.001 | 59.5 ± 0.1 | 1.182 ± 0.009 | 1.16 |

[a]$J_{SC}$: the short-circuit current intensity; [b]$V_{OC}$: the open-circuit voltage; [c]FF: the fill factor; [d]ECE: the electricity conversion efficiency; ECE obtained with a mask; [e]Relative ECE: the relative value of ECE of the experimental group against the control group. All average values are obtained from more than five measurements.

28.50 a.u./% RH (with an 80.78 times improvement, humidity: 37–74% RH), instant response, and enhanced reproducibility. The silk PCs can also be applied to enhance the ECE of semitransparent DSSCs (with a 16% improvement), which can be applied as smart shutters to convert sunlight into electricity. However, achieving fluorescence emission amplification by embedding PC "self-collimators" in silk materials is not the only purpose for this study; discovering promising applications of silk biomaterials in optical/electronic devices is another important goal. This method of complete control of fluorescence emission by introducing mesoscopic ordered structures and its applications will significantly broaden the utility of fluorescence in various fields, such as optical systems, optoelectronic technology, and biological sensors.

## Supporting Information

Supporting Information is available from the Wiley Online Library or from the author.

## Acknowledgements

## Conflict of Interest

The authors declare no conflict of interest.

## Keywords

[1] a) M. Baldo, M. Thompson, S. Forrest, *Nature* **2000**, *403*, 750; b) X. L. Li, G. Xie, M. Liu, D. Chen, X. Cai, J. Peng, Y. Cao, S. J. Su, *Adv. Mater.* **2016**, *28*, 4614; c) L. M. Smith, J. Z. Sanders, R. J. Kaiser, P. Hughes, C. Dodd, C. R. Connell, C. Heiner, S. B. Kent, L. E. Hood, *Nature* **1986**, *321*, 674.

[2] a) Y. Haga, K. Ishii, K. Hibino, Y. Sako, Y. Ito, N. Taniguchi, T. Suzuki, *Nat. Commun.* **2012**, *3*, 177; b) S. Impellizzeri, B. Mccaughan, J. F. Callan, F. M. Raymo, *J. Am. Chem. Soc.* **2012**, *134*, 2276; c) M. Heo, H. Cho, J. W. Jung, J. R. Jeong, S. Park, J. Y. Kim, *Adv. Mater.* **2011**, *23*, 5689.

[3] a) D. W. Piston, G.-J. Kremers, *Trends Biochem. Sci.* **2007**, *32*, 407; b) J. Homola, S. S. Yee, G. Gauglitz, *Sens. Actuators, B* **1999**, *54*, 3; c) S. Maenosono, *Chem. Phys. Lett.* **2003**, *376*, 666.

[4] a) R. Liu, Q. Deng, Z. Yang, D. Yang, M.-Y. Han, X. Y. Liu, *Adv. Funct. Mater.* **2016**, *26*, 5534; b) Y. Song, Z. Lin, L. Kong, Y. Xing, N. Lin, Z. Zhang, B. H. Chen, X. Y. Liu, *Adv. Funct. Mater.* **2017**, *27*, 1700628; c) N. B. Lin, F. Hu, Y. L. Sun, C. X. Wu, H. Y. Xu, X. Y. Liu, *Adv. Funct. Mater.* **2014**, *24*, 5284.

[5] a) T. Iizuka, H. Sezutsu, K. i. Tatematsu, I. Kobayashi, N. Yonemura, K. Uchino, K. Nakajima, K. Kojima, C. Takabayashi, H. Machii, *Adv. Funct. Mater.* **2013**, *23*, 5232; b) Y. Xing, C. Shi, J. Zhao, W. Qiu, N. Lin, J. Wang, X. B. Yan, W. D. Yu, X. Y. Liu, *Small* **2017**, *13*, 1702390; c) D. W. Kim, O. J. Lee, S.-W. Kim, C. S. Ki, J. R. Chao, H. Yoo, S.-i. Yoon, J. E. Lee, Y. R. Park, H. Kweon, *Biomaterials* **2015**, *70*, 48.

[6] N. Lin, X. Y. Liu, *Chem. Soc. Rev.* **2015**, *44*, 7881.

[7] S. Nishimura, N. Abrams, B. A. Lewis, L. I. Halaoui, T. E. Mallouk, K. D. Benkstein, d. L. J. Van, A. J. Frank, *J. Am. Chem. Soc.* **2003**, *125*, 6306.

[8] N. Lin, L. Cao, Q. Huang, C. Wang, Y. Wang, J. Zhou, X. Y. Liu, *Adv. Funct. Mater.* **2016**, *26*, 8885.

[9] P. Jiang, J. F. Bertone, K. S. Hwang, V. L. Colvin, *Chem. Mater.* **1999**, *11*, 2132.

[10] L. Bechger, P. Lodahl, W. L. Vos, *J. Phys. Chem. B* **2005**, *109*, 9980.

[11] a) C. Fu, D. Porter, Z. Shao, *Macromolecules* **2009**, *42*, 7877; b) Y. Y. Diao, X. Y. Liu, G. W. Toh, L. Shi, J. Zi, *Adv. Funct. Mater.* **2013**, *23*, 5373.

[12] F. Bella, G. Leftheriotis, G. Griffini, G. Syrrokostas, S. Turri, M. Grätzel, C. Gerbaldi, *Adv. Funct. Mater.* **2016**, *26*, 1127.

[13] E. M. Barea, J. Ortiz, F. J. Payá, F. Fernández-Lázaro, F. Fabregat-Santiago, A. Sastre-Santos, J. Bisquert, *Energy Environ. Sci.* **2010**, *3*, 1985.

[14] E. D. Kosten, J. H. Atwater, J. Parsons, A. Polman, H. A. Atwater, *Light: Sci. Appl.* **2013**, *2*, e45.